In–situ powder neutron diffraction study on the formation process of $LaMg_2NiH_7$

Toyoto Sato[a*], Kazutaka Ikeda[b], Motoaki Matsuo[c], Kazutoshi Miwa[d], Toshiya Otomo[b,e], Stefano Deledda[f], Bjørn C. Hauback[f], Guanqiao Li[g], Shigeyuki Takagi[a], Shin–ichi Orimo[a,g]

Affiliations

[a]Institute for Materials Research, Tohoku University, Japan

[b]Institute of Materials Structure Science, High Energy Accelerator Research Organization, Japan

[c]School of Science and Technology, Kwansei Gakuin University, Japan

[d]Toyota Central Research & Development Laboratories, Inc., Japan

[e]Department of Materials Structure Science, The Graduate University for Advanced Studies, Japan

[f]Physics Department, Institute for Energy Technology, Norway

[g]WPI–Advanced Institute for Materials Research, Tohoku University, Japan.

*Corresponding author. Tel.: +81– (0)22–215–2094; fax: +81–(0)22–215–2091.

E–mail: toyoto@imr.tohoku.ac.jp

Abstract

The formation process from the intermetallic compound $LaMg_2Ni$ to a complex hydride (deuteride) $LaMg_2NiD_7$ composed of La^{3+}, $2\times Mg^{2+}$, $[NiD_4]^{4-}$, and $3\times D^-$ was investigated by in–situ powder neutron diffraction under deuterium gas pressure at room temperature. Below 0.001 MPa, small amount of deuterium was initially dissolved in the lattice of $LaMg_2Ni$ forming $LaMg_2NiD_{0.05}$ and two new hydride phases ($LaMg_2NiD_{x1}$ and $LaMg_2NiD_{x2}$) were continuously yielded. Furthermore, $LaMg_2NiD_{4.6}$ with $NiD_{1.9}$ and $NiD_{3.3}$ units and interstitial deuterium atoms was formed prior to appearing of $LaMg_2NiD_7$. From their Bragg peak positions, the deuterium contents $x1$, and $x2$ were inferred as $0.05 < x1 < x2 < 4.6$. At approximately 0.001 MPa, $LaMg_2NiD_7$ started forming. Since the intermediate deuterides had similar metal atomic framework of $LaMg_2Ni$, we revealed that $LaMg_2NiD_7$ formation proceeded through multiple deuteride phases with maintaining of the metal atomic framework of $LaMg_2Ni$.

Keywords: In–situ powder neutron diffraction; Complex hydride; Crystal structure

Introduction

Complex hydrides are composed of metal cation(s) such as Li^+ and Mg^{2+} and complex anion(s) such as $[BH_4]^-$ and $[NiH_4]^{4-}$, in which the hydrogen atoms as ligand covalently bond to the central atom. The complex hydrides are attractive due to a wide variety of functionalities, such as hydrogen storage, superconductivity, fast ionic conductivity, magnetism, and metal–insulator transition [1–6].

Although the formation process of complex hydrides is of both fundamental and technological interest in order to further understand such functionalities, it remains incompletely understood because of the large accompanying reconstructions of the metal atomic frameworks. For instance, a complex hydride YMn_2H_6, in which Y is coordinated by four Mn ($[MnH_6]^{5-}$), is yielded from YMn_2, in which Y is coordinated by twelve Mn (Laves polyhedron) [7]. In contrast, the complex hydride $LaMg_2NiH_7$ reported by Yvon et al., composing of La^{3+}, $2\times Mg^{2+}$, $[NiH_4]^{4-}$, and $3\times H^-$, is formed from an intermetallic compound $LaMg_2Ni$ where the metal atomic framework of $LaMg_2Ni$ is maintained (Fig. 1) [8–11]. Then, the formation process of $LaMg_2NiH_7$ is suggested to infer from the atomic arrangements in the same manner that many interstitial hydrides have been investigated. From our recent investigations on the hydrogenation reaction of $LaMg_2Ni$, we discovered that $LaMg_2NiH_7$ formation was preceded by an intermediate phase $LaMg_2NiH_{4.6}$ [12]. Using powder neutron diffraction (PND) on a deuteride analog prepared in an ex–situ experiment, $LaMg_2NiH_{4.6}$ was elucidated to adopt a monoclinic crystal structure (a = 8.592 Å, b = 7.995 Å, c = 6.099 Å, and β = 99.318° in the space group $P2_1/m$ (No. 11)) with $NiH_{1.9}$ and $NiH_{3.3}$ units, and interstitial hydrogen atoms (see Fig. 1). The $NiH_{1.9}$ and $NiH_{3.3}$ units have similar atomic arrangements as the complex anion $[NiH_4]^{4-}$ in $LaMg_2NiH_7$. Using theoretical calculations, $LaMg_2NiH_{4.6}$ was confirmed to be a metallic hydride and the results showed to be the covalent bonding between Ni and H in the $NiH_{1.9}$ and $NiH_{3.3}$ units. Thus, the $NiH_{1.9}$ and $NiH_{3.3}$ units could be the basis for the formation of the complex anion $[NiH_4]^{4-}$ in $LaMg_2NiH_7$. Such units have also been reported in hydrides of rare earth and transition metals (e.g., $Ce_2Ni_7H_{4.7}$), $MgNi_2H_3$ and Pd–based complex hydrides (e.g., Li_2PdH_2) [13–19]. Since the $NiH_{1.9}$ and $NiH_{3.3}$ units were reminiscent of $[NiH_4]^{4-}$ and similar to their related hydrides, they were suggested to be precursors for formation of the complex anion $[NiH_4]^{4-}$ in our previous work [12].

In this study, we performed an in–situ PND experiment under deuterium gas pressure to directly observe and further elucidate details of the formation process from $LaMg_2Ni$ to $LaMg_2NiD_7$.

Experimental methods

$LaMg_2Ni$ was prepared by induction melting of a mixture of La ingots (Sigma–Aldrich, 99.9%) and Mg_2Ni powder (Kojundo Chemical Laboratory, 99.9%) in a molar ratio of 1:1. The details are described in ref. 12.

The in–situ PND experiment was performed at room temperature under deuterium gas pressure (<5 MPa) on the NOVA at the Material and Life Science Experimental Facility (MLF) of the Japan Proton Accelerator Research Complex (J–PARC), Japan. $LaMg_2Ni$ (1.8142 g) was filled in a cylindrical single–crystal sapphire sample container with an outside diameter and thickness of 10.8 mm and 2.5 mm, respectively. The deuterium gas was loaded to the cylindrical single–crystal sapphire sample container every 4 h and the deuterium gas pressure was gradually increased up to 5 MPa. In this paper, deuterium gas pressure refers to 4 h later after the deuterium loading. PND patterns were obtained from the detectors of medium resolution ($\Delta d/d \approx 0.6\%$) with the scattering angles $2\theta = 72-108°$ every 4 h. Subtraction of the contribution of the sample container was performed with separately measured diffraction data of container without sample. The detector pixels contain Bragg peaks of the single–crystal sapphire were identified and these pixels were not used in the data analysis. The PND patterns included the contribution from the sample container, which was separately observed by NOVA at room temperature, then subtracted.

The unit cell parameters were calculated by the indexing programs TREOR97 [20] and PIRUM [21] and the Rietveld analysis was performed using the GSAS software with the graphical interface EXPGUI (version 1.80) [22] on the PND data with d–spacing = 0.66 to 6.55 Å. Profile function developed by Von Dreele et al was used for the Rietveld analysis [23]. The background was modeled by 16–terms Chebyschev polynomial function model in GSAS.

The sample was handled in Ar or He gas filled glove boxes with a dew point below 183 K and with less than 1 ppm of O_2 to prevent (hydro–) oxidation.

Results and discussion

Figure 2 shows PND patterns under deuterium gas pressures from below 0.001 to 4.34 MPa at room temperature. The minimum measurable pressure is 0.001 MPa in this experiment. In this paper, we refer pressures lower than the minimum measurable pressure to below 0.001 MPa. The data are compared with the simulated PND patterns of $LaMg_2Ni$, $LaMg_2NiD_{4.6}$, and $LaMg_2NiD_7$, respectively. It is observed shifts in Bragg peak positions, new Bragg peaks appear, and Bragg peaks of $LaMg_2NiD_{4.6}$ and $LaMg_2NiD_7$ are observed already at deuterium pressure below 0.001 MPa and at room

temperature. These peak shifts and presence of new peaks were not observed in our previous ex–situ experiment [12]. This suggests that $LaMg_2Ni$ starts absorbing deuterium below 0.001 MPa and with changes in the crystal structure. The deuteration reaction temperature and pressure are much lower than in previous reports [8–12]. The remaining $LaMg_2NiD_{4.6}$, which is approximately 30 wt.% in the PND analyzed by the Rietveld refinement, at 4.34 MPa is attributed to the slow kinetics of the deuteration reaction from $LaMg_2NiD_{4.6}$ to $LaMg_2NiD_7$ at room temperature. This reaction was completed at higher temperatures in the hydride analog $LaMg_2NiH_{4.6}$.

The formation process from $LaMg_2Ni$ to $LaMg_2NiD_7$ proceeds by three steps; (1) an initial deuteration reaction starting immediately in 4 h after deuterium gas loading, (2) an intermediate reaction below 0.001 MPa (32 h later after deuterium gas loading), and (3) final formation above 0.001 MPa. In the (1) and (2) steps, pressures are below minimum measurable range (0.001 MPa). We first address the unit cell parameters of $LaMg_2Ni$ during (1) the initial deuteration reaction. The unit cell parameters of $LaMg_2Ni$ as a function of time after deuterium gas loading are plotted in Fig. 3 and they are listed in Table 1. Prior to deuterium gas loading, the Bragg peaks on the PND pattern are indexed by an orthorhombic unit cell with $a = 4.2120(5)$ Å, $b = 10.2626(14)$ Å, and $c = 8.3428(12)$ Å, which corresponds to $LaMg_2Ni$ [8, 9]. Following the deuterium gas loading, the *a*– and *c*–axes are slightly elongated and shortened respectively, while the *b*–axis is almost unchanged by dissolution of deuterium in the lattice of $LaMg_2Ni$. In order to clarify if deuterium atoms are dissolved in the lattice of $LaMg_2Ni$, Rietveld analysis on the PND pattern 4 h after deuterium gas loading was performed. The stoichiometry of the deuterium dissolved phase is determined as $LaMg_2NiD_{0.05}$ with deuterium located on a tetrahedral site coordinated by two La and two Mg atoms, and on a site coordinated by one La and two Mg atoms (the crystallographic parameters and Rietveld refinement fits are shown in Supplementary material). Such deuterium dissolved phases have also been reported in the initial deuteration reactions of the intermetallic compounds $LaNi_5$ and Mg_2Ni, which form $LaNi_5D_{0.3}$ [24] and $Mg_2NiD_{0.3}$ [25], respectively. The volume expansions is much smaller in $LaMg_2NiD_{0.05}$ (less than 0.1%) than in $LaNi_5D_{0.3}$ (0.4%) and $Mg_2NiD_{0.3}$ (4%). Even for the fully deuterided phases, the volume expansions in $LaMg_2NiD_7$ (19%) is significantly smaller than in $LaNi_5D_6$ (25%) and Mg_2NiD_4 (32%). In the initial intermetallics the distances between the metal atoms in $LaMg_2Ni$ is bigger than in $LaNi_5$ and Mg_2Ni. The shortest interatomic distances are listed in Table 2. This suggests that $LaMg_2Ni$ has more voids for accommodation of deuterium (hydrogen) atoms in the crystal structure than $LaNi_5$ and Mg_2Ni. Therefore, the lower volume expansion on deuteration (hydrogenation) reaction

of $LaMg_2Ni$ could originate from additional spaces in the crystal structures of the initial intermetallic compounds.

The next part is the deuteration reaction under deuterium gas pressure below 0.001 MPa after 4 h. In this deuterium gas pressure range, two new phases and $LaMg_2NiD_{4.6}$ are identified. Prior to $LaMg_2NiD_{4.6}$ formation, two unknown Bragg peaks appear at approximately d = 3.65 Å and 3.70 Å (marked by yellow and purple arrows, respectively, in Fig. 2). The Bragg peak at d = 3.65 Å appears before the peak at d = 3.70 Å, indicating that the two peaks originate from different phases. Here, we refer to the phases with peaks at d = 3.65 Å and d = 3.70 Å as $LaMg_2NiD_{x1}$ and $LaMg_2NiD_{x2}$, respectively. The Bragg peaks with weak intensities related to $LaMg_2NiD_{x1}$ and $LaMg_2NiD_{x2}$ are limited in number, and thus their crystal structures are difficult to elucidate. All observed Bragg peak positions of $LaMg_2NiD_{x1}$ and $LaMg_2NiD_{x2}$ in d–spacing = 0.66–8.05 Å are close and appear at lower d–spacing than for $LaMg_2NiD_{4.6}$. This suggests that $LaMg_2NiD_{x1}$, $LaMg_2NiD_{x2}$ and $LaMg_2NiD_{4.6}$ have similar crystal structures. Assuming the similarity of the crystal structures, the hydrogen contents of $LaMg_2NiD_{x1}$ and $LaMg_2NiD_{x2}$ are suggested to be $0.05 < x1 < x2 < 4.6$. At this stage of the reaction, the deuterium atoms in $LaMg_2NiD_{x1}$ and $LaMg_2NiD_{x2}$ could be located in interstitial sites close to the Ni atoms as $LaMg_2NiD_{4.6}$ (Fig. 1).

Above approximately 0.001 MPa, both $LaMg_2NiD_{x1}$ and $LaMg_2NiD_{x2}$ disappear and the deuteration reaction proceeds from $LaMg_2NiD_{4.6}$ to $LaMg_2NiD_7$. During the reaction, neither Bragg peak shifts nor unknown Bragg peaks are observed, indicating the direct formation of $LaMg_2NiD_7$ from $LaMg_2NiD_{4.6}$ under this condition. As mentioned above, $LaMg_2NiD_{4.6}$ and $LaMg_2NiD_7$ adopt similar metal atomic frameworks to $LaMg_2Ni$ (see Fig. 1). Thus, we have revealed that $LaMg_2NiD_7$ forms through multiple deuteride phases with similar metal frameworks of $LaMg_2Ni$.

Conclusions

We have performed an in–situ PND experiment at deuterium gas pressures below 5 MPa at room temperature. The experiment directly and precisely revealed the formation process from $LaMg_2Ni$ to $LaMg_2NiD_7$ composed of La^{3+}, $2\times Mg^{2+}$, $[NiD_4]^{4-}$, and $3\times D^-$. Even at room temperature, $LaMg_2Ni$ started absorbing deuterium below 0.001 MPa, forming a deuterium dissolved phase ($LaMg_2NiD_{0.05}$). Continuously, two new phases were identified ($LaMg_2NiD_{x1}$ and $LaMg_2NiD_{x2}$). After the formation of those deuteride phases, $LaMg_2NiD_{4.6}$ with $NiD_{1.9}$ and $NiD_{3.3}$ units, and interstitial deuterium atoms was formed. The Bragg peak positions of $LaMg_2NiD_{x1}$ and $LaMg_2NiD_{x2}$ implied that their crystal structures including deuterium atomic positions resembled that of

$LaMg_2NiD_{4.6}$, but with lower deuterium contents than $LaMg_2NiD_{4.6}$ ($0.05 < x1 < x2 < 4.6$). In the final reaction step, $LaMg_2NiD_{4.6}$ was formed into $LaMg_2NiD_7$. Thus, the in–situ PND experiment revealed that $LaMg_2NiD_7$ forms via multiple deuteride phases, in which the deuterium atoms were first dissolved in the lattice of $LaMg_2Ni$, then locate in the interstitial sites and around the Ni atoms, and finally become covalently bonded to Ni, forming the complex anion $[NiD_4]^{4-}$.

Highlight

- Formation process of a complex hydride (deuteride) $LaMg_2NiD_7$
- Crystal structure changes during the hydrogenation (deuteration) reaction
- In–situ powder neutron diffraction experiments under deuterium gas pressure

Acknowledgements

We are grateful for technical support from H. Ohmiya and N. Warifune. This work was supported by JSPS KAKENHI (Grant No. 16K06766, 16H06119 and 25220911) and Collaborative Research Center on Energy Materials in IMR (E–IMR). The neutron scattering experiment was approved by the Neutron Science Proposal Review Committee of J–PARC/MLF (Proposal No. 2014A0200).

References

[1] Orimo S, Nakamori Y, Eliseo JR, Züttel A, Jensen CM. Complex hydrides for hydrogen storage. Chem Rev 2007;107:4111–32.

[2] Sakintuna B, Lamari–Darkrim F, Hirscher M. Metal hydride materials for solid hydrogen storage: A review. Int J Hydrogen Energy 2007;32:1121–40.

[3] Eberle U, Felderhoff M, Schüth F. Chemical and physical solutions for hydrogen storage. Angew Chem Int Ed 2009;48:6608–30.

[4] Schouwink P, Ley MB, Tissot A, Hagemann H, Jensen TR, Smrčok L, Černý R. Structure and properties of complex hyride perovskite materials. Nat Commun 2014;5:5706.

[5] Unemoto A, Matsuo M, Orimo S. Complex hydrides for electrochemical energy storage. Adv Funct Mater 2014;24:2267–79.

[6] Takagi S, Orimo S. Recent progress in hydrogen–rich materials from the perspective of bonding flexibility of hydrogen. Scripta Mater 2015;109:1–5.

[7] Matsuo M, Miwa K, Semboshi S, Li H.–W, Kano M, Orimo S. First–principles studies of complex hydride YMn_2H_6 and its synthesis from metal hydride YMn2H4.6. Appl Phys Lett 2011;98:221908.

[8] Renaudin G, Guénée L, Yvon K. $LaMg_2NiH_7$, a novel quaternary metal hydride containing tetrahedral $[NiH_4]^{4-}$ complex and hydride ions. J Alloys Compd 2003;350:145–50.

[9] Yvon K, Renaudin G, Wei CM, Chou MY. Hydrogenation–induced insulating state in the intermetallic compound $LaMg_2Ni$. Phys Rev Lett 2005;94:066403.

[10] Di Chio M, Ziggiotti A, Baricco M, Effect of microstructure on hydrogen absorption in $LaMg_2Ni$. Intermetallics 2008; 16: 102–6.

[11] Xiao X, Liu G, Peng S, Yu K, Li S, Chen C, Chen L. Microstructure and hydrogen storage characteristic of nanocrystalline Mg + x wt% $LaMg_2Ni$ (x = 0–30) composites. Int J Hydrogen Energy 2010;35:2786–90.

[12] Miwa K, Sato T, Matsuo M, Ikeda K, Otomo T, Deledda S, Hauback BC, Li G, Takagi S, Orimo S. Metallic Intermediate Hydride Phase of $LaMg_2Ni$ with Ni−H Covalent Bonding: Precursor State for Complex Hydride Formation. J Phys Chem C 2016;120:5926–31.

[13] Bronger W. Complex transition metal hydrides. Angew Chem Int Ed Engl 1991;30:759–68.

[14] Yvon K. Complex transition–metal hydrides. Chimia 1998;52: 613–19.

[15] Olofsson–Mårtensson M Häussermann U, Tomkinson J, Noréus D. Stabilization of electron–dense palladium–hydrido complex in solid–state hydrides. J Am Chem Soc 2000;122:6960–70.
[16] Filinchuk YE, Yvon K, Emerich H. Tetrahedral D atom coordination of nickel and evidence for anti–isostructural phase transition in orthorhombic $Ce_2Ni_7D_{\sim 7}$. Inorg Chem 2007;46:2914–20.
[17] Yartys VA, Vajeeston P, Riabov AB, Ravindran P, Denys R, Maehlen JP, Delaplane RG, Fjellvåg H. Crystal chemistry and metal–hydrogen bonding in anisotropic and interstitial hydrides of intermetallics of rare earth (R) and transition metals (T), RT_3 and R_2T_7'. Z Kristallogr 2008;223:674–89.
[18] Yartys VA, Antonov VE, Beskrovnyy AI, Crivello J–C, Denys RV, Fedotov VK, Gupta M, Kulalov VI, Kuzovnikov MA, Latroche M, Morozov YG, Sheverev SG, Tarasov BP.Hydrogen–assisted phase transition in a trihydride $MgNiH_3$ synthesized at high H2 pressure: Thermodynamics, cystallgoraphic and electronic structures. Acta Mater 2015;82:316–27.
[19] Yartys VA, Antonov VE, Chernyshov D, Crivello J–C, Denys RV, Fedotov VK, Gupta M, Kulalov VI, Latroche M, Sheptyakov D. Structure and chemical bonding in MgNiH3 from combined high resolution synchrotron and neutron diffraction studies and ab initio electronic structure calculations. Acta Mater 2015;98:416–22.
[20] Werner P–E, Eriksson L. Westdahl M. TREOR, a semi–exhaustive trial–and–error powder indexing program for all symmetries. J Appl Crystallogr 1985;18:367–70.
[21] Werner P–E. A fortran program for least–squares refinement of crystal–structure cell dimensions. Ark Kemi 1969;31:513–6.
[22] Toby B.H. EXPGUI, A graphical user interface for GSAS. J Appl Crystallogr 2001;34:210–3.
[23] Von Dreele RB, Jorgensen JD, Windsor CG. Rietveld refinement with spallation neutron powder diffraction data. J Appl Crystallogr 1982;15:581–9.
[24] Fischer P, Furer A, Busch G, Schlapbach L. Neutron scattering investigations of the $LaNi_5$ hydrogen storage system. Helv Phys Acta 1977;50:421–30.
[25] Soubeyroux JL, Fruchart D, Mikou A, Pezat M, Darriet B. Etude structurale du systeme $Mg_2Ni–H_2$ I–La solution solide Mg_2NiH_x (x=0.30). Mat Res Bull 1984;19:895–904.

Table 1 Unit cell parameters of $LaMg_2Ni$ at the initial deuteration reaction. Estimation of unit cell parameters (32 h) are not allowed due to less number of the Bragg peaks.

Time (h)	*a* (Å)	*b* (Å)	*c* (Å)
0	4.2120(5)	10.2626(14)	8.3428(11)
4	4.2171(3)	10.2649(14)	8.3353(12)
8	4.2172(8)	10.2656(15)	8.3353(14)
12	4.2169(8)	10.2648(16)	8.3354(13)
16	4.2166(8)	10.2663(14)	8.3357(13)
20	4.2177(11)	10.2652(19)	8.3343(12)
24	4.2178(16)	10.2641(20)	8.3348(15)
28	4.2173(24)	10.2609(28)	8.3336(30)

Table 2 The shortest interatomic distances of each constituent element on $LaMg_2Ni$, $LaNi_5$ and Mg_2Ni

	$LaMg_2Ni$	$LaNi_5$	Mg_2Ni
La	2.95 Å (La–Ni)	2.90 Å (La–Ni)	
Mg	2.77 Å (Mg–Ni)		2.65 Å (Mg–Ni)
Ni	2.77 Å (Ni–Mg)	2.46 Å (Ni–Ni)	2.60 Å (Ni–Ni)

Figure captions

Figure 1 (Left) Crystal structures and (right) local atomic arrangements around Ni atom of (top) $LaMg_2Ni$, (middle) $LaMg_2NiH_{4.6}$ and (bottom) $LaMg_2NiH_7$ [8, 9, 12]. Gray, orange, green, blue circles indicate La, Mg, Ni and H, respectively.

Figure 2 Powder neutron diffraction patterns under deuterium gas pressure of < 5 MPa at room temperature. Black, green, red and blue lines indicate experimentally observed and simulated powder neutron patterns of $LaMg_2Ni$, $LaMg_2NiD_{4.6}$ and $LaMg_2NiD_7$, respectively. Bragg peaks of $LaMg_2NiD_{x1}$ and $LaMg_2NiD_{x2}$ are marked by yellow and purple arrows, respectively.

Figure 3 Unit cell parameters of $LaMg_2Ni$ as a function of time at the initial deuteration reaction. Estimation of unit cell parameters (32 h) are not allowed due to less number of the Bragg peaks.

Figure 1

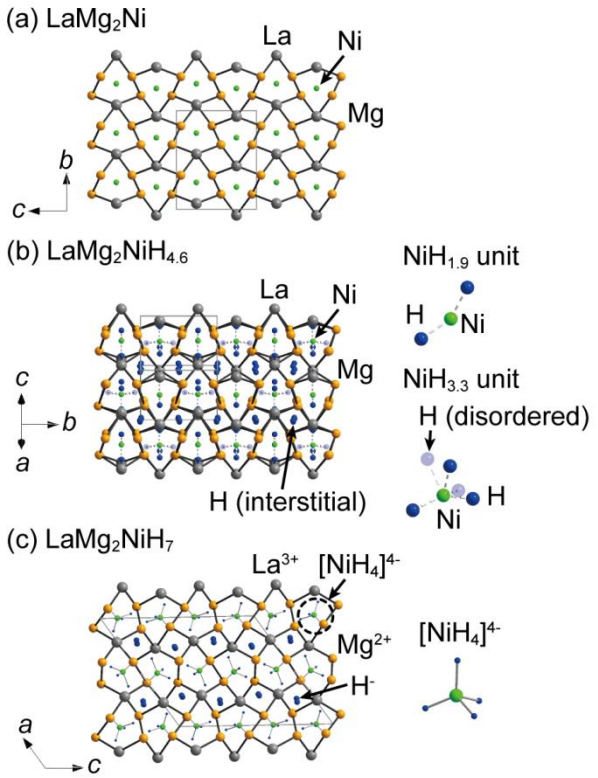

Figure 1 (Left) Crystal structures and (right) local atomic arrangements around Ni atom of (top) $LaMg_2Ni$, (middle) $LaMg_2NiH_{4.6}$ and (bottom) $LaMg_2NiH_7$ [8, 9, 12]. Gray, orange, green, blue circles indicate La, Mg, Ni and H, respectively.

Figure 2

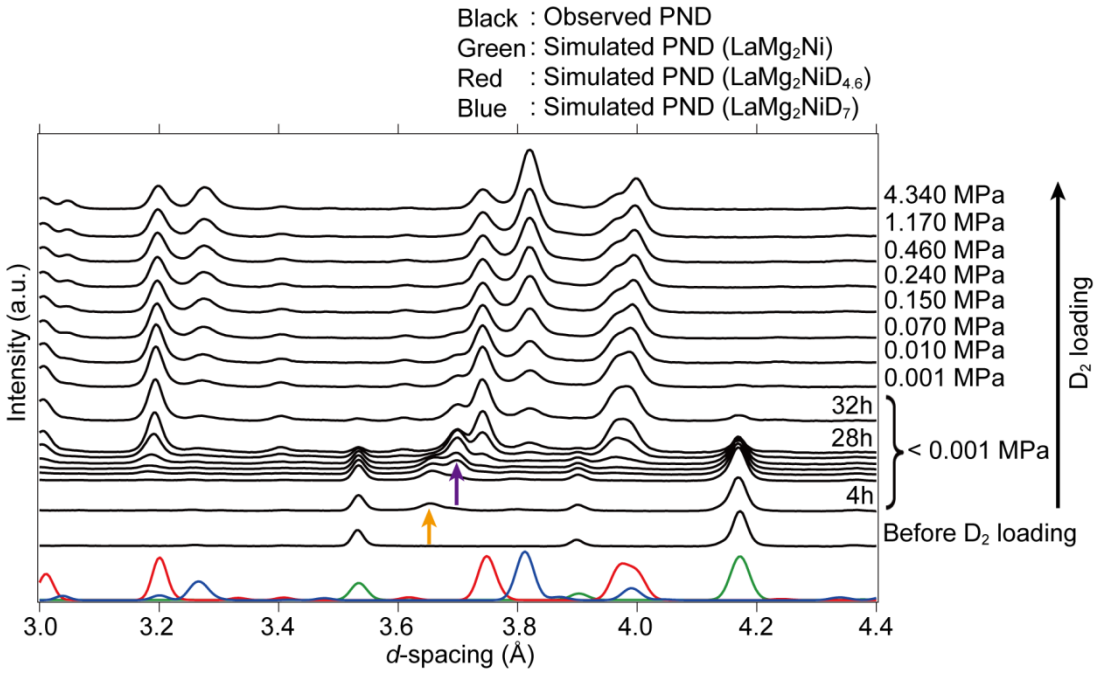

Figure 2 Powder neutron diffraction patterns under deuterium gas pressure of < 5 MPa at room temperature. Black, green, red and blue lines indicate experimentally observed and simulated powder neutron patterns of $LaMg_2Ni$, $LaMg_2NiD_{4.6}$ and $LaMg_2NiD_7$, respectively. Bragg peaks of $LaMg_2NiD_{x1}$ and $LaMg_2NiD_{x2}$ are marked by yellow and purple arrows, respectively.

Figure 3

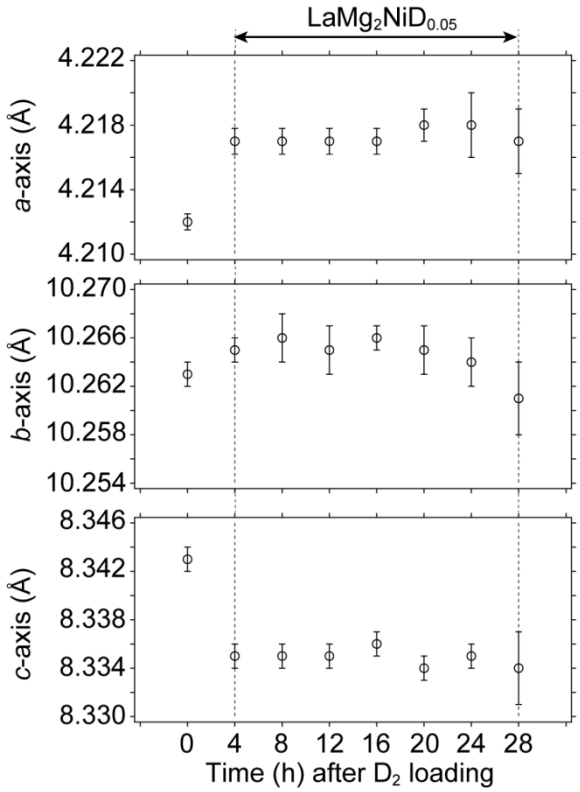

Figure 3 Unit cell parameters of $LaMg_2Ni$ as a function of time at the initial deuteration reaction. Estimation of unit cell parameters (32 h) are not allowed due to less number of the Bragg peaks.